Sensors & Diagnostics

Accepted Manuscript

This article can be cited before page numbers have been issued, to do this please use: S. Gallardo, B. King, S. G. Moorthy and B. H. Lessard, *Sens. Diagn.*, 2025, DOI: 10.1039/D5SD00103J.

View Article Online
DOI: 10.1039/D5SD00103J

Gate voltage effect on fluorinated and non-fluorinated copper phthalocyanine OTFT-based ammonia sensors

Sofia Gallardo[1], Banjamine King[1], Sujithkumar Ganesh Moorthy[1,2], Benoît H. Lessard[1,3*]

[1]*Department of Chemical and Biological Engineering, University of Ottawa, 161 Louis Pasteur, Ottawa, ON, Canada, K1N 6N5*
[2]*Department of Chemistry and Biomolecular Sciences, University of Ottawa, 150 Louis Pasteur, Ottawa, ON, Canada, K1N 6N5*
[3]*School of Electrical Engineering and Computer Science, University of Ottawa, 800 King Edward Ave, Ottawa, ON, Canada, K1N 6N5*

*Corresponding Authors: Benoit.Lessard@uottawa.ca (BHL)

Abstract

Organic thin-film transistors (OTFTs) have emerged as a promising platform for gas sensing applications due to their low-power operation, room-temperature sensitivity, and structural tunability. In this work, we investigate the effect of gate voltage (V_{GS}) on the ammonia (NH_3) sensing performance of OTFT-based sensors using copper phthalocyanine (CuPc, p-type) and its fluorinated derivative(F_{16}CuPc, n-type) as the active layers for the first time. Devices were exposed to NH_3 concentrations ranging from 0 to 100 ppm, and their electrical responses were monitored across different V_{GS} values. Results demonstrate that modulating V_{GS} significantly impacts key sensing parameters, including relative response (*RR*), sensitivity, limit of detection (LOD), and response/recovery kinetics. The lowest LODs achieved were 0.4 ppm for CuPc and 0.21 ppm for F_{16}CuPc. These findings highlight the potential of V_{GS} modulation as a powerful strategy to optimize OTFT sensor performance and provide a new dimension of tunability for gas detection technologies at room temperature.

Keywords: Organic thin-film transistors (OTFTs); ammonia gas sensor; copper phthalocyanine (CuPc); Copper(II) 1,2,3,4,8,9,10,11,15,16,17,18,22,23,24,25-hexadecafluoro-29H,31H-phthalocyanine(F_{16}CuPc); gate voltage modulation; response and recovery dynamics; limit of detection (LOD); room-temperature sensing; p-type and n-type semiconductors.

View Article Online
DOI: 10.1039/D5SD00103J

1. Introduction

Gas-sensing technologies have garnered significant attention in recent years due to their critical role in monitoring and controlling gas leaks, regulating indoor air quality, and managing humidity and CO_2 levels in congregate settings[1–3] . Gas sensors are also widely utilized for the detection of hazardous gases such as ammonia (NH_3), nitrogen dioxide (NO_2), and volatile organic compounds (VOCs), whose measurement are essential for environmental surveillance and occupational health monitoring[4]. Moreover, the development of gas sensor arrays with multivariate data analysis has opened pathways to non-invasive disease diagnostics, representing an emerging frontier in medical sensing technologies[5]. Consequently, the development of gas sensors that are highly sensitive, selective, and low power are critically important for both technological innovation and commercial deployment. Chemiresistors, typically composed of metal oxide sensing layers, have been widely deployed in gas sensing owing to their simplicity and high sensing performance[6,7]. However, the elevated operating temperatures of metal oxide sensors required to achieve their optimal performance (> 200 °C) poses a major barrier to seamless integration with standard silicon-based technologies[4] and makes them incompatible with low-power electronics [8].Organic semiconductor-based chemiresistors can operate at room temperature but only have two electrodes which limits their operational flexibility[9–12]. In contrast organic thin film transistors (OTFTs) based sensors, which are three terminal devices, are the combination of a sensor and an amplifier, a slight modulation in gate bias can change the response (signal-to-noise ratio) of the device by several orders of magnitude, which provides the potential for ultra-low limit of gas detection at room temperatutes[4,13–15], Additionally, organic semiconductors offer advantageous properties for sensing technologies, including low fabrication cost and synthetic tunability, which can enhance selectivity and sensitivity [16].

Recent advancement of OTFT-based gas sensors largely been driven by three core strategies: the development of novel organic semiconductors with enhanced sensitivity to target gases[17,18] , the systematic modification of interfacial properties between functional layers[19,20], and the precise control of the microstructural characteristics of the sensing films[12,13]. However, effect of modulating V_{GS} on sensor performance has been relatively unexplored. Shao et al. found that operating a TIPS-pentacene OTFT NO_2 sensor in the sub-threshold region resulted in a 19-fold increase in responsivity compared to operation in the saturation region [14]. Sato et al. demonstrated that the change of the Fermi level by manipulating the gate electric field in a graphene bilayer significantly affects not only the rate of molecular adsorption but also the carrier-scattering strength of adsorbed molecules[23]. However, a comprehensive analysis of gate voltage effect on other sensor performance metrics, such as sensitivity, limit of detection, response and recovery times is missing from the literature. As the V_{GS} is the principal controller of the charge carrier density, this intrinsic characteristic of

View Article Online
DOI: 10.1039/D5SD00103J

the OTFT architecture could justify the election of this more complicated architecture over a two-terminal device for specific applications.

Herein, we investigate the effect of V_{GS} on the gas sensing performance of OTFT-based NH_3 sensors with p-type organic semiconductor copper phthalocyanine (CuPc) and n-type organic semiconductor copper(II) 1,2,3,4,8,9,10,11,15,16,17,18,22,23,24,25-hexadecafluoro-29H,31H-phthalocyanine (F_{16}CuPc) as the sensing layers. NH_3 was selected as the target analyte due to its critical role across various sectors, including agricultural, pharmaceutical, and biomedical diagnostics[24], with over 175 million tonnes produced per year [25]. CuPc and F_{16}CuPc have been widely used in gas sensing platforms such as chemiresistors[26], OTFT[27,28] and heterojuctions[29–31]. However, to the best of our knowledge, these results demonstrate the first report of OTFT-based sensors using these materials as the sensing layer for NH_3 sensing . Devices were exposed to concentrations of NH_3 gas from 0 to 100 ppm, and the impact of V_{GS} on sensitivity, limit of detection (LOD), and response kinetics was systematically evaluated. Our approach demonstrates that modulating the operating V_{GS} serves as an effective strategy to enhance the performance of three-terminal gas sensors, and highlights the advantages offered by OTFTs.

2. Materials and methods

2.1 Device fabrication

N-Doped Si substrates (Ossila) with a 230 nm thermally grown SiO_2 dielectric layer were treated following the procedure reported in our previous work[32]. Bottom-gate top-contact (BGTC) OTFTs using CuPc and F_{16}-CuPc as the organic semiconductor were fabricated by thermally evaporating a 50 nm-thick layer at 0.2 Å·s^{-1} under vacuum ($P < 2 \times 10^{-6}$ Torr). Substrates were then removed, and a diamond-tipped pen was used to scratch the section of a substrate to yield exposed Si for gate electrode deposition. The substrates were then placed in a source-drain shadow mask ($L = 1$ mm, $W = 65$ μm) purchased from BlueRing. Electrodes were fabricated by thermally depositing a 50 nm-thick layer of Ag at a rate of 1 Å·s^{-1} under vacuum ($P < 2 \times 10^{-6}$ Torr).

View Article Online
DOI: 10.1039/D5SD00103J

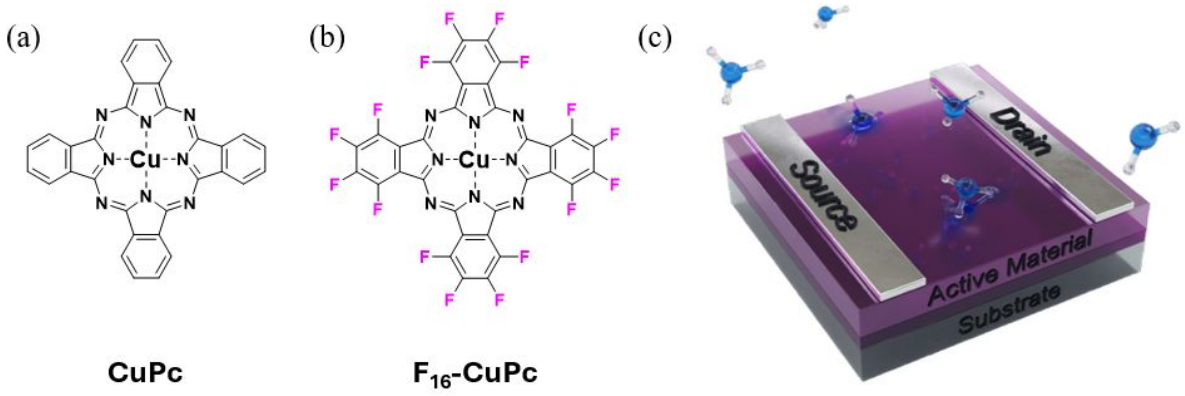

Figure 1. Molecular structure a) CuPc and b) F_{16}CuPc, c) OTFT sensor device scheme

2.2. Gas sensing set up and electrical characterization

A blend of NH_3 and synthetic air (1000 ppm NH_3, purchased from Messer Canada Inc, Canada) was diluted with dry synthetic air using mass flow controllers (total flow: 200 sccm to reach stable, controlled and adjustable ammonia concentrations from 0 to 100 ppm) prior to being mixed and introduced to a testing chamber containing the device under test. The final concentration of the gas and the relative humidity was controlled and monitored using a custom Labview program. The electrical characterization of the sensor was performed with a custom-built auto tester and a Keithley 2614B source meter previously reported by our group[32], allowing us to set the gate–source voltage and source–drain voltage (V_{SD}) while measuring the source–drain current (I_{DS}) in the device under test. The autotester was directly connected to the testing chamber, with autotester probes directly contacting the source, drain, and gate electrodes. For gas sensing experiments, the V_{GS} and V_{DS} was maintained constant while recording the I_{DS} under different NH_3 concentrations. Transfer and output curves were measured firstly under synthetics air, followed by measurements at different ammonia concentrations. Transfer curves were measured with the gate voltage sweeping between -10 and 45 V for F_{16}CuPc and from 10 to - 45 V for CuPc based devices. Both with a step size of 0.45 V, and a source–drain voltage (V_{DS}) of 45 V and - 45 V, respectively. Output curves were measured using a V_{DS} ranging between 45 and 0 V and V_{GS} varying from 0 to −45 V, with a step of 5 V and -5 V for F_{16}CuPc and CuPc respectively. The threshold voltage (V_{th}) and mobility (μ) were calculated from the transfer curves at the saturation regime using *Equation 1*.

$$Ids = \frac{\mu C_i W}{2L}(V_{GS} - V_{th})^2 \qquad \textit{Equation 1.}$$

where C_i is the capacitance of the dielectric layer, L and W represent the length and width of the channel, respectively.

View Article Online
DOI: 10.1039/D5SD00103J

3. Results and discussion

3.1 Effect of NH_3 on F_{16}CuPc and CuPc OTFT-based sensors performance

The transfer and output curves of the CuPc and F_{16}CuPc OTFTs measured under ambient conditions are shown in (**Figure 2 a-c**) and exhibit electrical characteristics consistent with previous research[27]**.** F_{16}CuPc has a (n-type) mobility of 0.02 cm/Vs and a V_{th} of 6.8 V and CuPc a (p-type) mobility of 0.01cm/Vs and a V_{th} of 6.4 V.

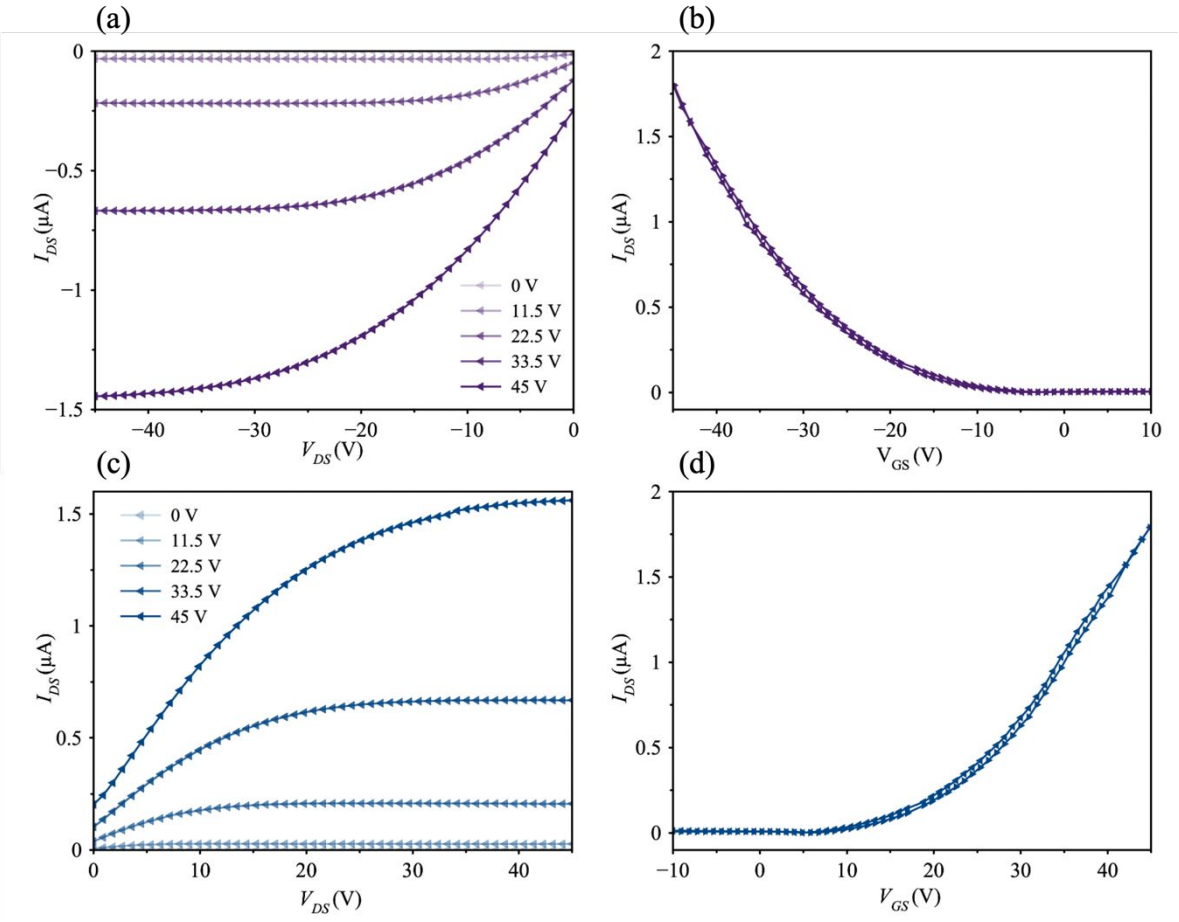

Figure 2 Output and transfer characteristics of CuPc (a, b) and F16CuPc (c, d) OTFTs. Transfer curves were measured at V_{DS}= −45 Vfor CuPc and V_{DS}= 45 V for F_{16}CuPc, with V_{GS} swept from 10 to –45 V and –10 to 45 V, respectively. Output curves were measured at V_{GS} of (0, -11.5, -22.5, -33.5 and -45) for CuPc and (0, 11.5, 22.5, 33.5 and -45) for F_{16}CuPc.

3.2 Operational V_{GS} effect on F_{16}CuPc and CuPc OTFT-based sensor's performance metrics

View Article Online
DOI: 10.1039/D5SD00103J

Devices were exposed to different concentrations of NH_3 varying from 0 to 100 ppm at a fixed flow rate of 200 SCCM. In-situ measurements of the transfer and output curves were taken using an exposure time (under NH_3) of 2 minutes at each step in concentration with a recovery time (under synthetic air) of 4 minutes. For CuPc sensors, I_{DS} decreases accompanied by a shift in V_T, under exposure to NH_3 and increases during the recovery period (**Figure 3 a** and b). The log plots of the transfer curve which more clearly highlights the shift in the V_T (**Figure 3b**). These observations are consistent with a p-type behaviour where NH_3 molecules donate electrons to the CuPc film, resulting in a depletion of holes and a decrease in I_{DS}. This is consistent with previously-reported CuPc chemiresistors which demonstrated p-type behaviour when exposed to NH_3[28]. Contrarily, I_{DS} increases upon exposure to NH_3 for F_{16}CuPc OTFT devices (**Figure 3d**) with a shift in V_T (**Figure 3e**), which is consistent with n-type behaviour, where an increase in electron carrier density in the film results in an increase in I_{DS}.

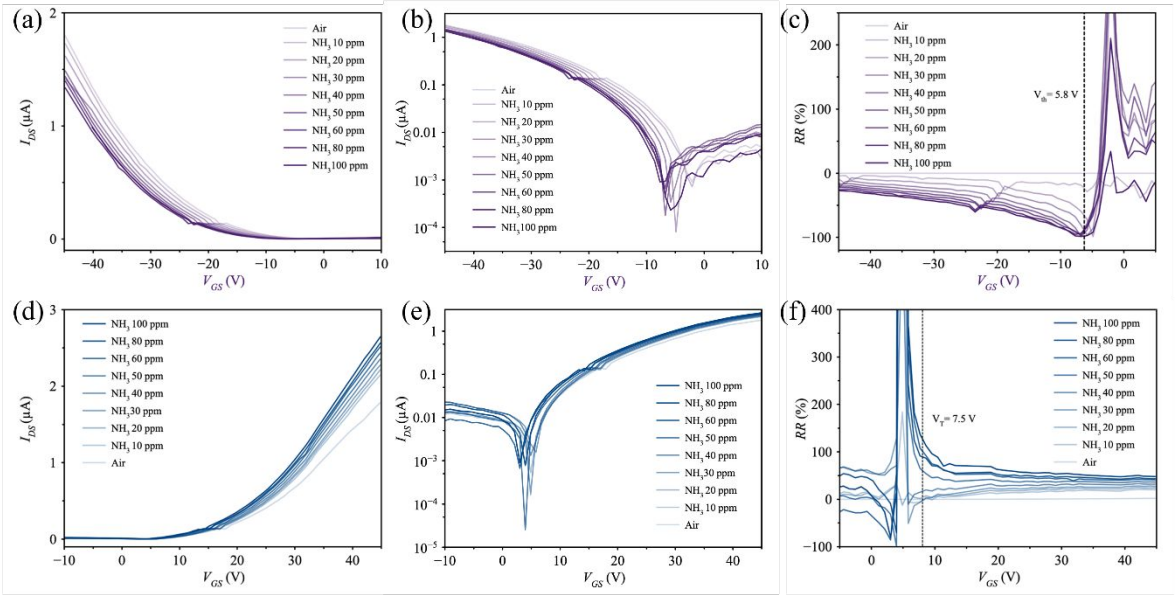

Figure 3 Transfer curves at different ammonia concentrations CuPc a) linear plot and b) log plot, and F_{16}CuPc d) linear plot and e) log plot. The relative response as a function of gate voltage for c) CuPc, f) F_{16}CuPc OTFTs as a function of ammonia concentrations.

A relation between the *RR* of the sensor and V_{GS} was established by plotting *RR* as a function of V_{GS} across the NH_3 concentrations we measured in this work (**Figure 3. c** and **f**). *RR* was calculated using *Equation 2*[33];

$$RR\,\% = \frac{I_f - I_0}{I_0} \times 100 \qquad \textit{Equation 2.}$$

View Article Online
DOI: 10.1039/D5SD00103J

where I_f and I_0 are the final and initial current values for each concentration. To be able to plot the *RR* across all the V_{GS} values, the I_f is equal to the transfer curve taken at the corresponding NH_3 concentration and I_0 is the transfer curve taken under synthetic air. By doing this, it's easier to visualize how the *RR* under the same NH_3 concentration can be increased or decreased just by operating the OTFT-based sensor on a different V_{GS} value.

For CuPc devices, the *RR* is negative, while for F_{16}CuPc the *RR* is positive which is consistent with the n-type and p-type behaviour shown before. For both materials, the highest *RR* is observed in the subthreshold region and is attributed to the filling of charge traps by the majority charge carriers[34]. Despite the high *RR* values in this region, 12000% for F_{16}CuPc and 4000% for CuPc, *RR* begins to behave linearly beyond the subthreshold region of the transfer curves. For CuPc the *RR* increases at lower V_{GS} for all measured NH_3 concentrations. The impact of the V_{GS} on the *RR* was more prominent at low NH_3 concentrations (10 ppm), *RR* increased from -3.5% to -18% when the V_{GS} was decreased from - 43 V to -8.6. Rather than high concentrations (100 ppm), where the *RR* increased from -27 % to -97 % when the V_{GS} was equally decreased. For F_{16}CuPc the effect of the V_{GS} on the *RR* is more dependent on the NH_3 concentration. For low concentrations (10 ppm) the *RR* is decreased when operating at lower V_{GS} but for high concentrations (100 ppm) it shows the opposite behaviour. These findings show the potential to optimize the sensor *RR* for specific NH_3 concentration windows by tuning the $V_{GS.}$

3.3 Dynamic measurements of the OTFT-based sensors

High sensitivity and low LOD are critical for evaluating the performance of OTFT-based ammonia sensors. To investigate the impact of gate voltage V_{GS} on the dynamic response, we exposed the devices to NH_3 concentrations ranging from 10 to 100 ppm, using 1-minute exposure and 4-minute recovery cycles. Measurements were performed at a constant drain-source voltage of +45 V for F_{16}CuPc and –45 V for CuPc, while systematically varying V_{GS}. Notably, all the V_{GS} measurements were performed on the same day in the same sensor to able to compare the results. **Figure 4. a–f** presents the time-resolved drain current under increasing NH_3 concentrations at different V_{GS} values. The sensitivity of each device was extracted from calibration curves, defined by the *RR* versus concentration. A clear trend emerged: both CuPc and F_{16}CuPc exhibited decreasing sensitivity at higher V_{GS} values. In the case of CuPc, a nonlinear and undetectable response at lower concentrations (10–20 ppm) was observed when operating at V_{GS} = −45 V. However, at V_{GS} = −36, the sensor displayed a linear and enhanced response, achieving a maximum sensitivity of 0.024% ppm^{-1} three orders of magnitude higher than previously reported for chemiresistor configurations[28]. Further reduction in V_{GS} to –22 V did not yield significant changes in sensitivity, suggesting saturation at this regime **(Table 1).**

In contrast, F_{16}CuPc demonstrated linear behavior across all gate biases, with notable improvement at lower V_{GS}. At V_{GS} =11, sensitivity increased by a factor of 33 compared to

View Article Online
DOI: 10.1039/D5SD00103J

operation at 45 V. This strong gate dependence underscores the tunability of OTFT-based sensors for optimizing performance parameters.

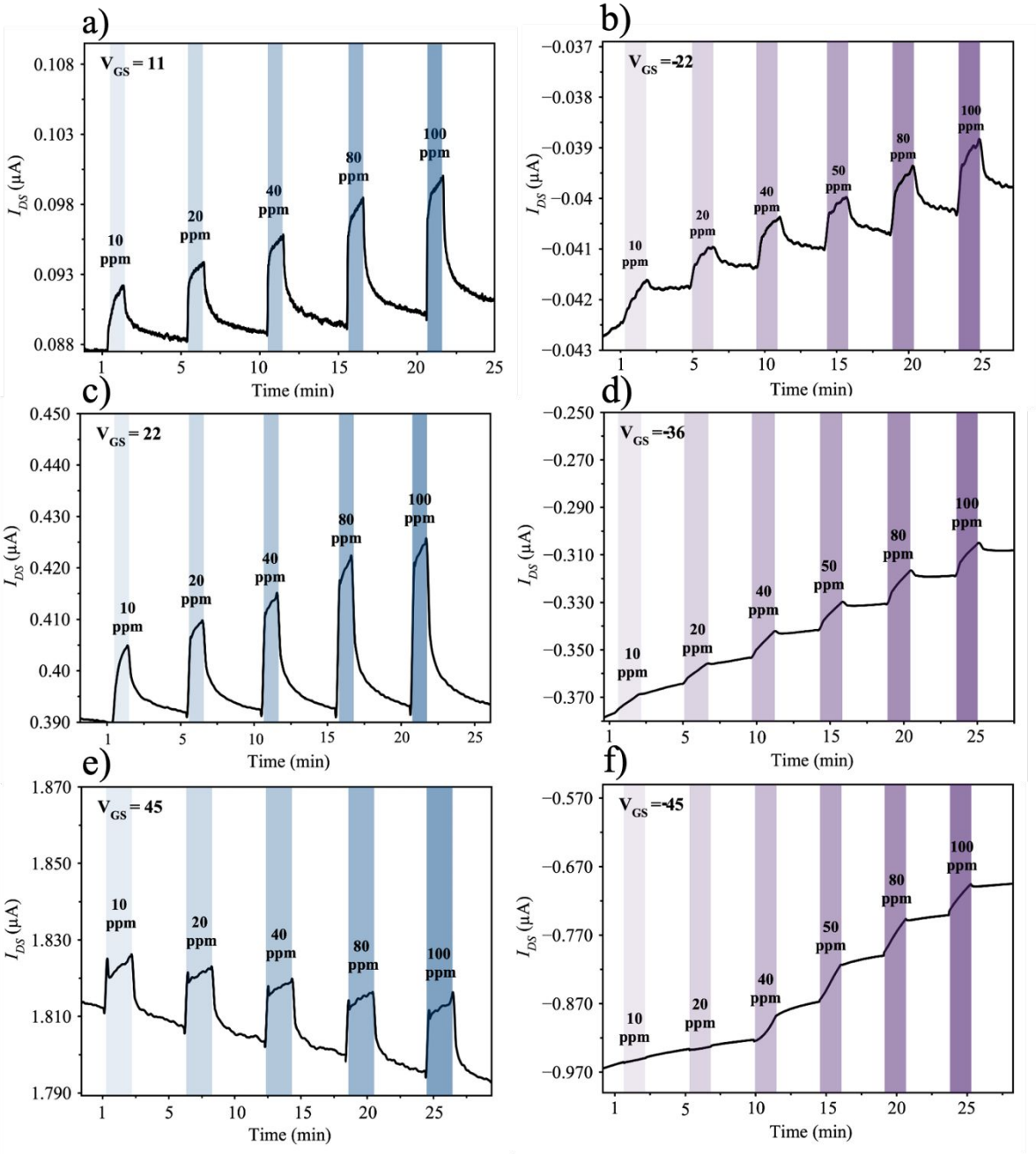

Figure 4. Response of OTFT sensors under successive exposure of NH_3 for 1 min and recovery under synthetic air for 4 min in the range of NH_3 concentration from 10 – 100 ppm in dry air and 20–22° at different V_{GS}. a), c) and e) F_{16}CuPc OTFT and b), d), f) CuPc OTFT. For F_{16}CuPc a V_{DS} = 45 V was used for all the measurements and for CuPc a V_{DS} = - 45 V.

View Article Online
DOI: 10.1039/D5SD00103J

To estimate the minimum detectable concentration, the LOD was calculated using *Equation 3*[33].

$$LOD = \frac{3N}{S \times I_0} \qquad \textit{Equation 3.}$$

where N is the standard deviation of the baseline current during the recovery period, SS is sensitivity (ppm^{-1}), and I_0 is the baseline current. The extracted LOD values are presented in **Table 1.**

Interestingly, although sensitivity decreases with increasing V_{GS}, lower LOD values are achieved at higher gate biases due to the larger baseline currents, which improve the signal-to-noise ratio. For CuPc, the LOD improved from 4.73 ppm at $V_{GS} = -22$ V to 0.4 ppm at $V_{GS} = -36$ V. However, is important to mention that the CuPc sensor operated at $V_{GS} = -36$ and $V_{GS} = -45$ don't show an appropriate recovery after exposure, limiting its sensing capabilities, therefore the values calculated for LOD and sensitivity are mentioned only for comparison reasons. A similar trend was observed for F_{16}CuPc, where the LOD decreased from 1.04 ppm at $V_{GS} = 45$ V to 0.21 ppm at $V_{GS} = 22$ V. As V_{GS} directly modulates the current in an OTFT architecture, the LOD can be tuned accordingly depending on the sensor´s application. By adjusting the gate bias, the sensor's baseline current and amplification characteristics change, enabling optimization for either high sensitivity or low detection thresholds based on specific environmental or industrial needs.

Table 1. Summary of gas sensing parameters as a function of V_{GS} for CuPc and F_{16}CuPc OTFT-based sensors.

Semiconductor	V_{GS} (V)	$S^{a)}$ (% ppm^{-1})	$LOD^{b)}$ (ppm)	*Res. time* [c)] (s)	*Rec. time* [c)] (s)
CuPc	22	-0.01	4.73	40.04	N/A
	36	-0.02*	0.40*	57.51	N/A
	45	N/A	N/A	60.08	N/A
F_{16}CuPc	11	0.1	0.53	30.70	180.52
	22	0.07	0.21	40.10	113.79
	45	0.003	1.042	33.76	102.98

[a)]*Sensitivity (S) is expressed as the percentage change in current per ppm of NH_3,* [b)] *LOD was calculated according to Equation 3, and* [c)] *response (Res) and recovery (Rec) times correspond to the time to reach 90% signal change. N/A indicates cases where the current did not recover to 90% of its initial value or the value could not be calculated. *Under these conditions, no recovery was observed for the sensor upon exposure to NH_3.*

View Article Online
DOI: 10.1039/D5SD00103J

Baseline drift remains a critical challenge in the practical deployment of OTFT-based gas sensors, often limiting device stability and long-term reliability even for encapsulated OTFTs[34,35]. This drift is primarily associated with incomplete desorption of analytes during the recovery phase, as well as charge trapping effects induced by prolonged gate bias. While strategies such as thermal desorption or pulsed gating have been shown to mitigate drift in various FET-based sensing platforms[36], they typically require additional circuitry or temperature control that complicate device integration. In contrast, our results demonstrate that modulation of the gate voltage alone can mitigate baseline drift in OTFT sensors operating at room temperature, offering a practical and low-power approach for performance enhancement.

Recovery and response times were calculated from the same short-exposure experiments used to evaluate sensitivity and LOD. The response time is defined here as the time required for the drain current I_{DS} to reach 90% of its maximum value after exposure to NH_3, while the recovery time corresponds to the time required for I_{DS} to return to 90% of its baseline following analyte removal. In both CuPc and F_{16}CuPc-based devices, response time showed limited dependence on gate bias. For F_{16}CuPc, the response time ranged from 30.7 s at V_{GS} = 11 V to 33.76 s at V_{GS} = 45 V, indicating minimal influence of gate modulation on the response dynamics. CuPc devices showed a slightly different behavior, where the fastest response (40.04 s) was observed at the lowest measured V_{GS} of 22 V.

Recovery behavior exhibited a clear dependence on gate bias, particularly for F_{16}CuPc-based devices. At V_{GS} = 11 V, a positive drift in baseline current was observed (**Figure. 4 e**), likely due to incomplete NH_3 desorption. Despite this, the sensor successfully returned to 90% of its baseline signal within a recovery time of 180.52 s, indicating effective recovery even under low gate bias conditions. When operated at V_{GS} = 45 V, the baseline drift reversed to a negative direction (**Figure. 4 c**), likely reflecting stronger bias stress effects; however, the recovery was faster, reaching 90% recovery in 102.98 s. Notably, at an intermediate bias of V_{GS} = 22 V, the sensor exhibited minimal drift and a recovery time of 113.79 s. This intermediate behavior suggests a compensatory effect in which incomplete desorption and electrical stress-induced degradation balance out.

CuPc-based devices, by contrast, did not reach 90% recovery within the measurement window at any applied V_{GS}. The baseline drift was consistently negative, indicating persistent charge trapping and limited desorption. Notably, operating at lower V_{GS} values reduced the extent of current drift (**Figure. 4 b,d**), suggesting reduced bias stress, but this was not sufficient to enable full recovery. These results reinforce the material-dependent nature of OTFT sensor recovery, highlighting the role of semiconductor-analyte interactions and electrical stress tolerance.

4. Conclusion

We successfully fabricated highly sensitive OTFT-based NH_3 sensors employing CuPc and F_{16}CuPc as sensing layer for the first time and systematically investigated the influence of V_{GS} on their response kinetics and detection limit. Modulation of V_{GS} proved to be a simple yet highly effective approach to enhance sensor characteristics for both materials.

View Article Online
DOI: 10.1039/D5SD00103J

Specifically, reducing V_{GS} significantly improved sensitivity of F_{16}CuPc sensors, increasing by a factor of 33 when switching the V_{GS} from 45 V to 11 V, reaching a maximum sensitivity of 0.1 (% ppm^{-1}). For CuPc sensors, the *RR* to low NH_3 concentrations (10 and 20 ppm) was initially negligible but was improved to 2.1% and 2.3%, respectively, achieving a maximum sensitivity of 0.02 (% ppm^{-1}). We also demonstrate that the LOD was also influenced by tuning V_{GS}, where a larger applied V_{GS} yielded lower LOD values, with CuPc exhibiting a reduction by an order of magnitude 4.73ppm to 0.4 ppm, and F_{16}CuPc displaying a twofold decrease 0.5 ppm to 0.2 ppm. This improvement is attributed to an enhanced signal-to-noise ratio, which can be finely controlled through V_{GS} modulation in OTFT architectures.

We also demonstrated the response and recovery kinetics were influenced by V_{GS}, CuPc-based devices showed moderate response times (40–60 s), but failed to recover 90% of their initial current after NH_3 exposure. In contrast, F_{16}CuPc devices exhibited faster response times (31–40 s) and significantly better recovery, with 90% current recovery in 103 s by increasing the V_{GS} from 11 to 45 V. These differences were related to the baseline drift and adsorption-desorption behaviors specific to each material. Overall, this work highlights V_{GS} modulation as a powerful strategy to improve the sensitivity and dynamic response of OTFT-based gas sensors and provides a highly effective pathway for the design of highly tunable, application-oriented sensing platforms.

Acknowledgement
We thank Natural Sciences and Engineering Research Council of Canada (NSERC) Discovery program (RGPIN-04079-2020 to B.H.L) for supporting this project and NSERC CGS to B.K. We thank the Canadian Foundation for Innovation, CFI# 40178 (HIIT) and CFI# 43247 (SSMART), for support in acquisition and maintenance of the infrastructure needed for this project. The authors would like to express their sincere gratitude to Franco Ziroldo, Gérard Nina, and Patrick Pageau for their invaluable assistance in the design and construction of the gas sensing setup. We would like to thank Dr. Joseph G. Manion (CGFigures) for providing a figure element

References

1. Rothschild A, Komem Y. The effect of grain size on the sensitivity of nanocrystalline metal-oxide gas sensors. *J Appl Phys*. 2004;95(11):6374-6380. doi:10.1063/1.1728314
2. S. KM, Jose AS, K. P, Chowdhury P, Barshilia HC. Sputter deposited p-NiO/n-SnO2 porous thin film heterojunction based NO2 sensor with high selectivity and fast response. *Sens Actuators B Chem*. 2020;310:127830. doi:10.1016/j.snb.2020.127830
3. Maheswari S, Karunakaran M, Kasirajan K, Bruno Chandrasekar L, Boomi P. Yttrium - Substituted SnO2 thin films and its gas sensing activity against NH3 gas: Characterization and sensitivity evaluation. *Sens Actuators Phys*. 2020;315:112303. doi:10.1016/j.sna.2020.112303
4. Singh AK, Chowdhury NK, Roy SC, Bhowmik B. Review of Thin Film Transistor Gas Sensors: Comparison with Resistive and Capacitive Sensors. *J Electron Mater*. 2022;51(5):1974-2003. doi:10.1007/s11664-022-09485-y
5. Khan S, Ali S, Bermak A. Recent Developments in Printing Flexible and Wearable

View Article Online
DOI: 10.1039/D5SD00103J

Sensing Electronics for Healthcare Applications. *Sensors*. 2019;19(5):1230. doi:10.3390/s19051230
6. Kumar A, Meunier-Prest R, Lesniewska E, Bouvet M. Interplay of electrode geometry and bias on charge transport in organic heterojunction gas sensors. *Sens Actuators B Chem*. 2022;369:132313. doi:10.1016/j.snb.2022.132313
7. Bengasi G, Meunier-Prest R, Baba K, et al. Molecular Engineering of Porphyrin-Tapes/Phthalocyanine Heterojunctions for a Highly Sensitive Ammonia Sensor. *Adv Electron Mater*. 2020;6(12):2000812. doi:10.1002/aelm.202000812
8. Zhang C, Xu K, Liu K, Xu J, Zheng Z. Metal oxide resistive sensors for carbon dioxide detection. *Coord Chem Rev*. 2022;472:214758. doi:10.1016/j.ccr.2022.214758
9. Di Zazzo L, Ganesh Moorthy S, Meunier-Prest R, et al. Ammonia and Humidity Sensing by Phthalocyanine–Corrole Complex Heterostructure Devices. *Sensors*. 2023;23(15):6773. doi:10.3390/s23156773
10. Ivanova V, Klyamer D, Tunç G, et al. Films of substituted zinc phthalocyanines as active layers of chemiresistive sensors for ammonia detection. *New J Chem*. 2023;47(42):19633-19645. doi:10.1039/D3NJ03400C
11. King B, Moorthy SG, Lesniewska E, Meunier-Prest R, Bouvet M, Lessard BH. Modulating the majority charge carrier type and performance of organic heterojunction ammonia sensors by increasing peripheral fluorination of the silicon phthalocyanine sublayer. *Sens Actuators B Chem*. 2024;408:135507. doi:10.1016/j.snb.2024.135507
12. Van Duy L, Thi Nguyet T, Hung CM, et al. Light-assisted room temperature ammonia gas sensor based on porphyrin-coated V2O5 nanosheets. *Sens Actuators B Chem*. 2024;409:135582. doi:10.1016/j.snb.2024.135582
13. Yan F, and Tang H. Application of thin-film transistors in label-free DNA biosensors. *Expert Rev Mol Diagn*. 2010;10(5):547-549. doi:10.1586/erm.10.50
14. Shao B, Liu Y, Zhuang X, et al. Crystallinity and grain boundary control of TIPS-pentacene in organic thin-film transistors for the ultra-high sensitive detection of NO2. *J Mater Chem C*. 2019;7(33):10196-10202. doi:10.1039/C9TC01219B
15. Song Z, Liu G, Tang Q, Zhao X, Tong Y, Liu Y. Controllable gas selectivity at room temperature based on Ph5T2-modified CuPc nanowire field-effect transistors. *Org Electron*. 2017;48:68-76. doi:10.1016/j.orgel.2017.05.043
16. Ganesh Moorthy S, King B, Kumar A, Lesniewska E, Lessard BH, Bouvet M. Molecular Engineering of Silicon Phthalocyanine to Improve the Charge Transport and Ammonia Sensing Properties of Organic Heterojunction Gas Sensors. *Adv Sens Res*. 2023;2(3):2200030. doi:10.1002/adsr.202200030
17. Flexible Graphene-Based Wearable Gas and Chemical Sensors | ACS Applied Materials & Interfaces. Accessed April 21, 2025. https://pubs.acs.org/doi/10.1021/acsami.7b07063
18. Wen F, Dillen DC, Kim K, Tutuc E. Shell morphology and Raman spectra of epitaxial Ge−SixGe1−x and Si−SixGe1−x core-shell nanowires. *J Appl Phys*. 2017;121(23):234302. doi:10.1063/1.4985616
19. Shi W, Yu J, Katz HE. Sensitive and selective pentacene-guanine field-effect transistor sensing of nitrogen dioxide and interferent vapor analytes. *Sens Actuators B Chem*. 2018;254:940-948. doi:10.1016/j.snb.2017.07.198
20. Huang W, Zhuang X, Melkonyan FS, et al. UV–Ozone Interfacial Modification in Organic Transistors for High-Sensitivity NO2 Detection. *Adv Mater*. 2017;29(31):1701706. doi:10.1002/adma.201701706

View Article Online
DOI: 10.1039/D5SD00103J

21. Santos AG, da Rocha GO, de Andrade JB. Occurrence of the potent mutagens 2-nitrobenzanthrone and 3-nitrobenzanthrone in fine airborne particles. *Sci Rep*. 2019;9(1):1. doi:10.1038/s41598-018-37186-2
22. Jiang Y, Huang W, Zhuang X, Tang Y, Yu J. Thickness modulation on semiconductor towards high performance gas sensors based on organic thin film transistors. *Mater Sci Eng B*. 2017;226:107-113. doi:10.1016/j.mseb.2017.08.019
23. Sato Y, Takai K, Enoki T. Electrically controlled adsorption of oxygen in bilayer graphene devices. *Nano Lett*. 2011;11(8):3468-3475. doi:10.1021/nl202002p
24. Shetty SS, Jayarama A, Bhat S, Satyanarayan, Karunasagar I, Pinto R. A review on metal-oxide based trace ammonia sensor for detection of renal disease by exhaled breath analysis. *Mater Today Proc*. 2022;55:113-117. doi:10.1016/j.matpr.2021.12.411
25. Ammonia: zero-carbon fertiliser, fuel and energy store.
26. Chia LS, Du YH, Palale S, Lee PS. Interaction of Copper Phthalocyanine with Nitrogen Dioxide and Ammonia Investigation Using X-ray Absorption Spectroscopy and Chemiresistive Gas Measurements. *ACS Omega*. 2019;4(6):10388-10395. doi:10.1021/acsomega.8b02108
27. Boileau NT, Melville OA, Mirka B, Cranston R, Lessard BH. P and N type copper phthalocyanines as effective semiconductors in organic thin-film transistor based DNA biosensors at elevated temperatures. *RSC Adv*. 2019;9(4):2133-2142. doi:10.1039/C8RA08829B
28. Chia LS, Du YH, Palale S, Lee PS. Interaction of Copper Phthalocyanine with Nitrogen Dioxide and Ammonia Investigation Using X-ray Absorption Spectroscopy and Chemiresistive Gas Measurements. *ACS Omega*. 2019;4(6):10388-10395. doi:10.1021/acsomega.8b02108
29. Huang W, Besar K, LeCover R, Rule AM, Breysse PN, Katz HE. Highly sensitive NH3 detection based on organic field-effect transistors with tris(pentafluorophenyl)borane as receptor. *J Am Chem Soc*. 2012;134(36):14650-14653. doi:10.1021/ja305287p
30. Fan H, Shi W, Yu X, Yu J. High performance nitrogen dioxide sensor based on organic field-effect transistor utilizing ultrathin CuPc/PTCDI-C8 heterojunction. *Synth Met*. 2016;211:161-166. doi:10.1016/j.synthmet.2015.11.021
31. Mateos M, Meunier-Prest R, Suisse JM, Bouvet M. Modulation of the organic heterojunction behavior, from electrografting to enhanced sensing properties. *Sens Actuators B Chem*. 2019;299:126968. doi:10.1016/j.snb.2019.126968
32. Ewenike RB, King B, Battaglia AM, et al. Toward Weak Epitaxial Growth of Silicon Phthalocyanines: How the Choice of the Optimal Templating Layer Differs from Traditional Phthalocyanines. *ACS Appl Electron Mater*. 2023;5(12):7023-7033. doi:10.1021/acsaelm.3c01389
33. King B, H. Lessard B. Review of recent advances and sensing mechanisms in solid-state organic thin-film transistor (OTFT) sensors. *J Mater Chem C*. 2024;12(16):5654-5683. doi:10.1039/D3TC03611A
34. Haneef HF, Zeidell AM, Jurchescu OD. Charge carrier traps in organic semiconductors: a review on the underlying physics and impact on electronic devices. *J Mater Chem C*. 2020;8(3):759-787. doi:10.1039/C9TC05695E
35. Zilker SJ, Detcheverry C, Cantatore E, de Leeuw DM. Bias stress in organic thin-film transistors and logic gates. *Appl Phys Lett*. 2001;79(8):1124-1126. doi:10.1063/1.1394718
36. Yang RD, Park J, Colesniuc CN, Schuller IK, Trogler WC, Kummel AC. Ultralow

View Article Online
DOI: 10.1039/D5SD00103J

drift in organic thin-film transistor chemical sensors by pulsed gating. *J Appl Phys*. 2007;102(3):034515. doi:10.1063/1.2767633

View Article Online
DOI: 10.1039/D5SD00103J

Data Availability Statement:

All data necessary to support the conclusions of this study are provided in the manuscript and the Electronic Supplementary Information (ESI). Additional information is available from the corresponding author upon reasonable request.